Theoretical study on the static performance of piezoelectric ceramic-polymer composites with 1-3 connectivity

Wenwu Cao, Q. M. Zhang, and L. E. Cross
Materials Research Laboratory, The Pennsylvania State University, University Park, Pennsylvania 16802

(Received 6 July 1992; accepted for publication 2 September 1992)

Inhomogeneous displacement profiles have been derived for a single-rod composite and a single-tube 1-3 ceramic-polymer composite under both uniaxial and hydrostatic stress. The effective piezoelectric constants for the composites have been derived in terms of the ceramic content, the piezoelectric and elastic constants of each component, and the aspect ratio of the ceramic rod. The stress concentration inside both phases is derived from the calculated inhomogeneous displacement profiles. It is found that only a finite portion of the polymer in the vicinity of the ceramic-polymer interface actually contributes to the stress transfer, and the induced additional stress on the ceramic also has a higher magnitude near the interface. The theoretical results quantitatively predict the performance of a given 1-3 structure, and can be used to optimize the design parameters, such as ceramic content, aspect ratio of the ceramic rods, rod geometry and rod arrangement, resin hardness, etc., for 1-3 structures designed for specific purposes.

I. INTRODUCTION

With the increasing application of piezoelectric composite structures, quantitative description of their physical properties has become a necessity for proper structural design. The most frequently encountered piezocomposites are 2-2- and 1-3-type ceramic-polymer composites. The names of these composites are defined according to their connectivities.[1] In the past, theoretical studies on this subject have been limited to the isostrain models.[2–4] Although the isostrain models can provide some general guidelines, their theoretical predictions are often larger than the experimental values.[5] In addition, the effect of the aspect ratio, which is proven experimentally to be a critical parameter in the 1-3 composite structure, is not included in the isostrain models. After analyzing the essential characteristics of the problem we have presented in a previous paper a theoretical model for the 2-2 composites.[6] This model can quantitatively describe the effective piezoelectric properties of the 2-2-type composites. In this paper we extend the model to address the 1-3-type composites which are more attractive and have much wider applications than the 2-2 structures from a practical point of view.

The fundamental physics in the 1-3 composites is the same as that in the 2-2-type composites. We expect the displacement profile in a 1-3 composite to be inhomogeneous under a prescribed stress field or an electric field because the two components have different elastic and piezoelectric properties. The difference between the 2-2 and 1-3 problems is the dimensionality, i.e., one-dimensional for the 2-2 type and two dimensional for the 1-3 type. Besides the dimensionality difference, there are two more complications in the 1-3-type composites: one is the geometry of the cross section of the ceramic rod, which is commonly chosen to be square or circular due to manufacturing convenience; the other is the rod arrangement in the composite, which usually is made into square or triangular configurations. Because the rod geometry and the rod arrangement define the boundary conditions for the problem, each case must be treated separately. Here we only solve two simple cases for which analytic solutions exist; using these two examples we wish to derive the essential features of the 1-3 structure and demonstrate the general procedure for dealing with the 1-3 composites. Solutions for an arbitrary rod geometry and rod arrangement may be calculated numerically.

The two cases to be treated are composites made of a single cylindrical ceramic rod and a single ceramic cylinder with a polymer matrix of finite dimension as shown in Figs. 1 and 2, respectively. One can think of them as the "unit cells" of a 1-3 composite. For simplicity, the outer boundary of the composite is also defined to be circular. Obviously, such a unit cell cannot be used to fill the whole space. However, it is a reasonable approximation to the composite with triangularly arranged ceramic rods (for which the unit cell has hexagonal symmetry) and, as will be proven later, at low ceramic content the results for the single-rod composite can even be used for composites with other rod arrangements.

II. DISPLACEMENT PROFILE IN A SINGLE-ROD COMPOSITE UNDER UNIAXIAL AND HYDROSTATIC STRESSES

The basic idea for constructing the static equilibrium condition is to single out the effective component of the displacement field. For the single-rod (tube) system as shown in Fig. 1 (Fig. 2), we choose a cylindrical coordinate system (r,ϕ,z) with the z and r directions along the axis of the ceramic rod (tube) and the radial direction, respectively, and ϕ as the angular variable. When the ce-

 0021-8979/92/245814-08$04.00

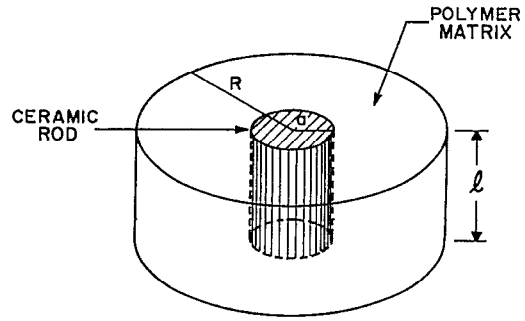

FIG. 1. A single ceramic rod composite of length l. The radius of the composite is R and a is the radius of the ceramic rod.

ramic rods are poled in the axial direction (the z direction in our calculations), the stress transfer in the 1-3 structure only enhances the piezoelectric response of the ceramic rods in the z direction. Therefore, to a good approximation, we only need to derive the z component of the displacement field. Following the procedure described in Ref. 6, we use the ansatz $u(r,z)=(2z/l)u(r,l/2)$, for the z component of the displacement field; then, under a uniaxial stress T_3 the static equilibrium condition for the polymer and ceramic phases can be written in the following form in a cylindrical coordinate system:

$$\frac{\mu^p l}{4}\left(\frac{\partial^2 u(r,l/2)}{\partial r^2}+\frac{1}{r}\frac{\partial u(r,l/2)}{\partial r}+\frac{1}{r^2}\frac{\partial^2 u(r,l/2)}{\partial \phi^2}\right)$$
$$=\frac{2Y^p}{l}u(r,l/2)-T_3, \quad r>a, \tag{1a}$$

$$\frac{c_{44}l}{4}\left(\frac{\partial^2 v(r,l/2)}{\partial r^2}+\frac{1}{r}\frac{\partial v(r,l/2)}{\partial r}+\frac{1}{r^2}\frac{\partial^2 v(r,l/2)}{\partial \phi^2}\right)$$
$$=\frac{2}{ls_{33}}v(r,l/2)-T_3, \quad r<a, \tag{1b}$$

where $u(r,l/2)$ and $v(r,l/2)$ are the z components of the displacement for the polymer and the ceramic, respectively, at the top surface of the composite. μ^p and Y^p denote the shear and Young's moduli of the polymer phase, and

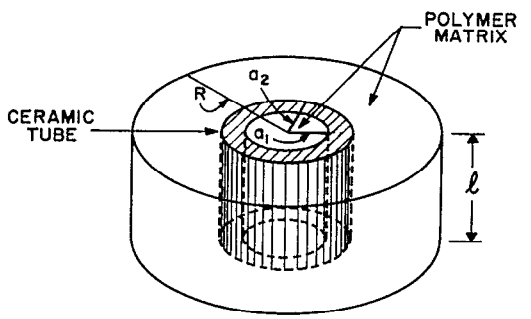

FIG. 2. A single ceramic tube composite of length l. The radius of the composite is R, while a_1 and a_2 are the inner and outer radii of the ceramic tube.

c_{44} and s_{33} are the shear elastic stiffness and the normal elastic compliance of the ceramic, respectively.

Considering the composite shown in Fig. 1, the solution must be independent of ϕ because of the symmetry, which means that the second derivative with respect to ϕ vanishes. By making the following substitution

$$\bar{u}=u(r,l/2)-(lT_3/2Y^p), \tag{2a}$$

$$\rho=r/\xi^p, \quad \xi^p=(l/2)\sqrt{\mu^p/2Y^p}, \tag{2b}$$

Eq. (1a) can be recast to the following zeroth-order Bessel equation of imaginary argument:

$$\rho^2\frac{\partial^2\bar{u}}{\partial\rho^2}+\rho\frac{\partial\bar{u}}{\partial\rho}-\rho^2\bar{u}=0. \tag{3}$$

Standard solutions exist for Eq. (3) so that the surface displacement of the polymer phase, $u(r,l/2)$, can be obtained using Eqs. (2a) and (2b),

$$u\left(r,\frac{l}{2}\right)=AK_0\left(\frac{r}{\xi^p}\right)+BI_0\left(\frac{r}{\xi^p}\right)+\frac{l}{2Y^p}T_3 \quad (r>a) \tag{4}$$

where $K_0(\rho)$ and $I_0(\rho)$ are the zeroth-order modified Bessel functions, and A and B are the constants of integration.

Similarly we can obtain the surface displacement profile for the ceramic rod by solving Eq. (1b) using the same technique,

$$v(r,l/2)=CI_0(r/\xi^c)+(l/2)s_{33}T_3 \quad (r<a), \tag{5}$$

where $\xi^c=l/2\sqrt{s_{33}c_{44}/2}$. Note that in Eq. (5) we have used the boundary condition that $v(r,l/2)$ is finite at $r=0$, so that only one integration constant C remains.

In order to determine the integration constants in the solutions Eqs. (4) and (5), three boundary conditions are needed. The first one can be obtained from the nonslip interface condition at $r=a$, viz.

$$u(a,l/2)=v(a,l/2). \tag{6}$$

The second one is the free-boundary condition at $r=R$ for the polymer phase,

$$\left.\frac{\partial u(r,l/2)}{\partial r}\right|_{r=R}=0 \tag{7}$$

[the derivative of $u(r,z)$ along the direction normal to the unit-cell boundary must always vanish in the composite structure due to symmetry]. For the single-rod composite in Fig. 1 we can use Newton's third law to derive the other condition needed to determine the constants as described

TABLE I. Elastic, piezoelectric, and dielectric constants of PZT5H[a] and epoxy[b] used in our calculations. ϵ_0 is the dielectric constant of vacuum.

PZT5H: $s_{33}=0.0208$ (10^{-9} m^2/N), $c_{44}=20.0$ (10^9 N/m^2), $\sigma^c=0.31$, $d_{33}=593$ (10^{-12} C/N), $d_{31}=-274$ (10^{-12} C/N), $\epsilon^c=3400\epsilon_0$
Epoxy: $Y^p=3.1$ (10^9 N/m^2), $\mu^p=1.148$ (10^9 N/m^2), $\sigma=0.35$, $\epsilon^p=3.5\epsilon_0$

[a]See Ref. 7.
[b]See Ref. 8.

in Ref. 6, but for later convenience, we use the following equivalent but more general boundary condition:

$$\mu^p \frac{\partial u(r,l/2)}{\partial r}\bigg|_{r=a} = c_{44} \frac{\partial v(r,l/2)}{\partial r}\bigg|_{r=a}. \tag{8}$$

Equation (8) states that the shear stress is a continuous function of r across the interface in the nonslip interface composite structures.

Now the three integration constants A, B, and C can be determined from Eqs. (6), (7), and (8); they are

$$A=\frac{-(l/2)I_1(\rho_R^p)I_1(\rho_a^c)(1/Y^p-s_{33})T_3}{\sqrt{(Y^p s_{33}\mu^p/c_{44})}I_0(\rho_a^c)[I_1(\rho_R^p)K_1(\rho_a^p)-I_1(\rho_a^p)K_1(\rho_R^p)]+I_1(\rho_a^c)[I_1(\rho_R^p)K_0(\rho_a^p)+K_1(\rho_R^p)I_0(\rho_a^p)]}, \tag{9a}$$

$$B=\frac{(l/2)K_1(\rho_R^p)I_1(\rho_a^c)(1/Y^p-s_{33})T_3}{\sqrt{(Y^p s_{33}\mu^p/c_{44})}I_0(\rho_a^c)[I_1(\rho_R^p)K_1(\rho_a^p)-I_1(\rho_a^p)K_1(\rho_R^p)]+I_1(\rho_a^c)[I_1(\rho_R^p)K_0(\rho_a^p)+K_1(\rho_R^p)I_0(\rho_a^p)]}, \tag{9b}$$

$$C=\frac{(l/2)[I_1(\rho_R^p)K_1(\rho_a^p)-I_1(\rho_a^p)K_1(\rho_R^p)](1/Y^p-s_{33})T_3}{I_0(\rho_a^c)[I_1(\rho_R^p)K_1(\rho_a^p)-I_1(\rho_a^p)K_1(\rho_R^p)]+\sqrt{(c_{44}/Y^p s_{33}\mu^p)}I_1(\rho_a^c)[I_1(\rho_R^p)K_0(\rho_a^p)+K_1(\rho_R^p)I_0(\rho_a^p)]}, \tag{9c}$$

where

$$\rho_a^p=a/\xi^p, \quad \rho_R^p=R/\xi^p, \quad \rho_a^c=a/\xi^c,$$

and $K_0(\rho)$, $I_0(\rho)$, $K_1(\rho)$, and $I_1(\rho)$ are the zeroth- and first-order modified Bessel functions.

Because of the coupling between the two components at the interface in the 1-3 structure, the total effective stress on the ceramic becomes larger but inhomogeneous. The magnitude of the effective total stress is the largest at the interface and becomes smaller away from the interface. The effective induced electric displacement in the ceramic now becomes

$$D(r)=d_{33}T_3^{\text{eff}}=\frac{d_{33}}{s_{33}}\frac{v(r,l/2)}{l/2}, \quad r<a. \tag{10}$$

From Eq. (10) we can calculate the total bound charge Q produced at the top surface of the ceramic rod,

$$Q=2\pi\int_0^a D(r)r\,dr=\gamma d_{33}T_{33}\pi a^2, \tag{11}$$

where

$$\gamma=1+\frac{(l/a)I_1(\rho_a^c)[I_1(\rho_R^p)K_1(\rho_a^p)-I_1(\rho_a^p)K_1(\rho_R^p)](1/Y^p-s_{33})}{\sqrt{(2s_{33}/c_{44})}I_0(\rho_a^c)[I_1(\rho_R^p)K_1(\rho_a^p)-I_1(\rho_a^p)K_1(\rho_R^p)]+\sqrt{(2/Y^p\mu^p)}I_1(\rho_a^c)[I_1(\rho_R^p)K_0(\rho_a^p)+K_1(\rho_R^p)I_0(\rho_a^p)]} \tag{12}$$

is the stress amplification factor.

We can see that the amplification factor depends on the elastic properties of both phases, the ceramic content $V_c=a^2/R^2$, and more important, the aspect ratio a/l. In order to visualize this aspect ratio dependence, we have calculated the numerical values of Eq. (12) for a PZT5H-epoxy composite using the input data in Table I. (PZT5H is a trademark of Vernitron Corp. for its lanthanum-doped PZT product.) The results are shown in Fig. 3. Two important conclusions can be drawn from the results in Fig. 3 as follows.

(i) There is a saturation value for the enhancement effect for any given aspect ratio a/l. This is because the stress transfer effect is limited only to the portion near the ceramic-polymer interface; in other words, only the polymer portion near the interface actually contributes to the enhancement effect. This point will be elaborated below. This saturation value of γ can be derived from Eq. (12) by taking the limit $R\to\infty$,

$$\lim_{R\to\infty}\gamma=1+\frac{(l/a)K_1(\rho_a^p)I_1(\rho_a^c)(1/Y^p-s_{33})}{\sqrt{(2s_{33}/c_{44})}I_0(\rho_a^c)K_1(\rho_a^p)+\sqrt{(2/Y^p\mu^p)}I_1(\rho_a^c)K_0(\rho_a^p)}. \tag{13}$$

This limiting value depends very strongly on the aspect ratio of the ceramic rod a/l, which may be visualized from the results shown in Fig. 3 at $V_c=0$; it decreases rapidly with the increase of the ratio a/l. The inclusion of the aspect ratio is one of the novel features of the current model.

(ii) The γ value obtained from the current model is always smaller than the isostrain result but larger than the two-phase decoupling result ($\gamma=1$, which can be obtained by taking the limit $a\to\infty$ for a finite l), depending on the aspect ratio a/l of the structure. In general, for a fixed ceramic content, thin and long rods should be used in order to get larger γ. The isostrain models actually give the upper limit for the enhancement factor, which can be derived from Eq. (12) for a finite R by taking the limit $l\to\infty$,

$$\lim_{l\to\infty}\gamma=\frac{1}{V_c+V_pY^ps_{33}}, \tag{14}$$

where V_c and V_p are the volume fractions of the ceramic and polymer respectively. Equation (14) is just the isostrain result.[9]

In order to see how the stress transfer actually takes place, the generated additional stress T_{add} inside both the ceramic and the polymer phases for a single-rod composite is calculated using the parameters from Table I. For clarity and simplicity, we assume $R\to\infty$ (corresponding to $V_c\to 0$); then the solutions for the z component of the displacement field inside the composite become

$$u(r,z)=\frac{z}{l/2}\left(AK_0(\rho^p)+\frac{l/2}{Y^p}T_3\right),\quad r>a, \tag{15a}$$

$$v(r,z)=\frac{z}{l/2}\left(CI_0(\rho^c)+\frac{l}{2}s_{33}T_3\right),\quad r<a, \tag{15b}$$

where

$$A=\frac{(l/2)I_1(\rho_a^c)(s_{33}-1/Y^p)T_3}{\sqrt{(Y^ps_{33}\mu^p/c_{44})}I_0(\rho_a^c)K_1(\rho_a^p)+I_1(\rho_a^c)K_0(\rho_a^p)}, \tag{16a}$$

$$C=\frac{(l/2)K_1(\rho_a^p)(1/Y^p-s_{33})T_3}{I_0(\rho_a^c)K_1(\rho_a^p)+\sqrt{(c_{44}/Y^ps_{33}\mu^p)}I_1(\rho_a^c)K_0(\rho_a^p)}. \tag{16b}$$

In this case the generated additional stress T_{add} is

$$T_{\text{add}}=T_3^{\text{eff}}-T_3=\begin{cases}\dfrac{I_1(\rho_a^c)(s_{33}Y^p-1)T_3K_0(\rho^p)}{\sqrt{(Y^ps_{33}\mu^p/c_{44})}I_0(\rho_a^c)K_1(\rho_a^p)+I_1(\rho_a^c)K_0(\rho_a^p)}, & r>a, \quad (17a)\\[2ex] \dfrac{K_1(\rho_a^p)(1/Y^ps_{33}-1)T_3I_0(\rho^c)}{I_0(\rho_a^c)K_1(\rho_a^p)+\sqrt{(c_{44}/Y^ps_{33}\mu^p)}I_1(\rho_a^c)K_0(\rho_a^p)}, & r<a. \quad (17b)\end{cases}$$

T_{add} is plotted in Fig. 4 for a single-rod PZT5H-epoxy composite with $a=0.5$, $l=2.5$ and 5, respectively. We can see that T_{add} has opposite signs in the ceramic ($r<0.5$) and in the polymer ($r>0.5$), and the magnitude is the largest at the interface. There is a substantial increase of the effective stress in the ceramic at the expense of the stress reduction in the polymer phase. Because of the difference between the elastic properties in the two phases, T_{add} subsides very fast away from the interface in the polymer but changes relatively slowly in the ceramic phase. Also, we note in Fig. 4 that T_{add} depends very strongly on the ratio a/l. With the increase of l, more polymer will participate in the stress transfer process. Although the maximum stress magnitude at the interface $a=0.5$ becomes slightly smaller, the total force transferred to the ceramic rod, which is the product of the stress and the surface area of the participating polymer, becomes larger. We found that the inhomogeneity of the additional stress becomes stronger as the a/l ratio increases.

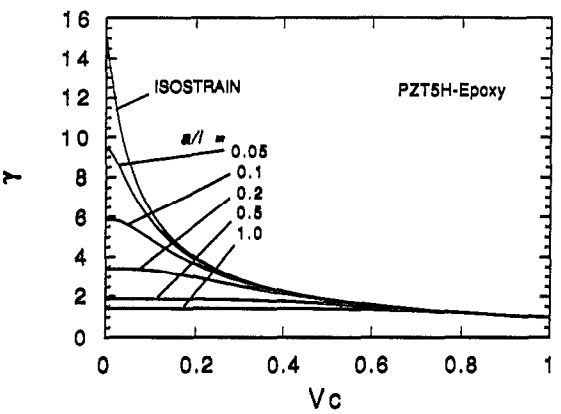

FIG. 3. Calculated dependence of the amplification factor γ on the ceramic content for a PZT5H-epoxy composite with the following aspect ratio: $a/l=0.05$, 0.1, 0.2, 0.5, and 1.0. The uppermost line is the isostrain result.

It is clear from the stress analysis that the most effective portion of the 1-3 structure is near the ceramic-polymer interface, especially for relatively large a/l ratio. Therefore, one of the fundamental guidelines for the structural design of 1-3 composite is to increase the ceramic-polymer interface area.

We now proceed to calculate the hydrostatic piezoelectric constant for the single-rod 1-3 composite shown in Fig. 1. The boundary condition for this problem should be constant stress on all surfaces of the composite. However, this boundary condition is not satisfied in the previous theoretical models which assumed isostrain boundary condition in the axial direction of the rods. Therefore, the effective hydrostatic piezoelectric constant of the 1-3 structure calculated from the previous models is often much larger than the experimental values.[5,9] The simple parallel model and series model could not give the right result because the conditions of isostrain in the z direction and equal stress in the x and y directions are self-contradictory. When stresses are applied in the x and y directions, the induced displacement in the z direction will be quite different in the ceramic and polymer phases, due to the difference in elastic com-

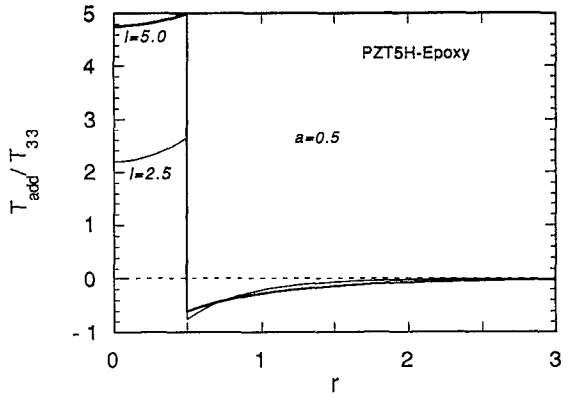

FIG. 4. Concentration of the generated additional stress T_{add} as a function of r for a single-rod PZT5H-epoxy 1-3 composite under a uniaxial stress T_3. The radius of the ceramic rod is 0.5. The thick line is for $l=5$ and the thin line for $l=2.5$. The maximum value of the additional stress appears at the interface $r=0.5$, and the signs of the stresses in the two phases are opposite.

pliance. Although the series model may be used in the x and y direction, the equal strain model must not be used in the z direction unless infinitely stiff plates are placed on the two surfaces of the composite. In order to adequately calculate the hydrostatic piezoelectric constant for the 1-3 composite, one must consider all three dimensions simultaneously and the solution should satisfy equal stress boundary conditions in all three dimensions.

Before we calculate the effective hydrostatic piezoelectric constant of the composite structure, let us discuss briefly the physics involved in the 1-3 structure. Equation (1) may be rewritten in the following form:

$$\frac{2}{l}u\left(r,\frac{l}{2}\right)=s_{33}^{p}\left[T_3+\frac{\mu^p l}{4}\left(\frac{\partial^2 u(r,l/2)}{\partial r^2}+\frac{1}{r}\frac{\partial u(r,l/2)}{\partial r}+\frac{1}{r^2}\frac{\partial^2 u(r,l/2)}{\partial\phi^2}\right)\right], \tag{18}$$

where $s_{33}^{p}=1/Y^p$ is the normal elastic compliance of the polymer. Equation (18) tells us that, in the composite, the effective T_3^{eff} [in the square bracket of Eq. (18)] is inhomogeneous due to the additional stress generated by the nonslip ceramic-polymer interface, although the applied stress T_3 is homogeneous. While in the other two dimensions, there is no interface enhancement effect, the stress will still be homogeneous, but the stresses applied in the directions perpendicular to the z direction can generate additional stress in the z direction due to the Poisson's ratio effect and the difference of elastic compliance in the two phases. When normal stresses are applied in all three dimensions, the local strain-stress relation in the z direction inside the polymer may be written as

$$\frac{2}{l}u\left(r,\frac{l}{2}\right)=s_{33}^{p}\left[T_3+\frac{\mu^p l}{4}\left(\frac{\partial^2 u(r,l/2)}{\partial r^2}+\frac{1}{r}\frac{\partial u(r,l/2)}{\partial r}+\frac{1}{r^2}\frac{\partial^2 u(r,l/2)}{\partial\phi^2}\right)\right]+s_{31}^{p}T_1+s_{31}^{p}T_2. \tag{19}$$

For the case of hydrostatic pressure, $T_1=T_2=T_3=-P$, Eq. (19) becomes

$$\frac{\mu^p l}{4}\left(\frac{\partial^2 u(r,l/2)}{\partial r^2}+\frac{1}{r}\frac{\partial u(r,l/2)}{\partial r}+\frac{1}{r^2}\frac{\partial^2 u(r,l/2)}{\partial\phi^2}\right)=\frac{2Y^p}{l}u\left(r,\frac{l}{2}\right)+(1-2\sigma)P, \tag{20}$$

where $\sigma=s_{31}^{p}/s_{33}^{p}$ is the Poisson's ratio for the polymer. Equation (20) is identical to Eq. (1a) if we replace T_3 with $-(1-2\sigma)P$. Similarly one can reach the same conclusion for the ceramic phase, except in this case we must replace T_3 by $-(1-2\sigma^c)P$, with $\sigma^c=s_{31}^{c}/s_{33}^{c}$.

Now the electric displacement in the ceramic under a hydrostatic pressure can be written as

$$D(r)=d_{33}\left[T_3+\frac{c_{44}l}{4}\left(\frac{\partial^2 v(r,l/2)}{\partial r^2}+\frac{1}{r}\frac{\partial v(r,l/2)}{\partial r}+\frac{1}{r^2}\frac{\partial^2 v(r,l/2)}{\partial\phi^2}\right)\right]+d_{31}T_1+d_{32}T_2$$
$$=d_{33}\left(\frac{2v(r,l/2)}{ls_{33}^{c}}-2\sigma^c P\right)-2d_{31}P. \tag{21}$$

Equation (21) includes both the Poisson's ratio effect and the interface enhancement.

From Eq. (11) the total charge Q produced by the hydrostatic pressure P can be obtained by integrating Eq. (21) over the end surface of the ceramic rod,

$$Q=-\pi a^2(\gamma_h d_{33}+2d_{31})P, \tag{22}$$

where

$$\gamma_h=1+\frac{(l/a)I_1(\rho_a^c)[I_1(\rho_R^p)K_1(\rho_a^p)-I_1(\rho_a^p)K_1(\rho_R^p)][(1-2\sigma)/Y^p-(1-2\sigma^c)s_{33}]}{\sqrt{(2s_{33}/c_{44})}I_0(\rho_a^c)[I_1(\rho_R^p)K_1(\rho_a^p)-I_1(\rho_a^p)K_1(\rho_R^p)]+\sqrt{(2/Y^p\mu^p)}I_1(\rho_a^c)[I_1(\rho_R^p)K_0(\rho_a^p)+K_1(\rho_R^p)I_0(\rho_a^p)} \tag{23}$$

is the amplification factor in the hydrostatic situation. Compared to Eq. (12), the only difference is the inclusion of the Poisson's ratio effect, i.e., the two factors $(1-2\sigma)$ and $(1-2\sigma^c)$.

From Eq. (22) the effective hydrostatic piezoelectric constant $\overline{d_h}$ of the composite is therefore given by

$$\overline{d_h}=(\gamma_h d_{33}+2d_{31})(a^2/R^2)=V_c(\gamma_h d_{33}+2d_{31}), \tag{24}$$

where V_c is the volume fraction of the ceramic. Equation (24) is plotted in Fig. 5 for several different aspect ratios

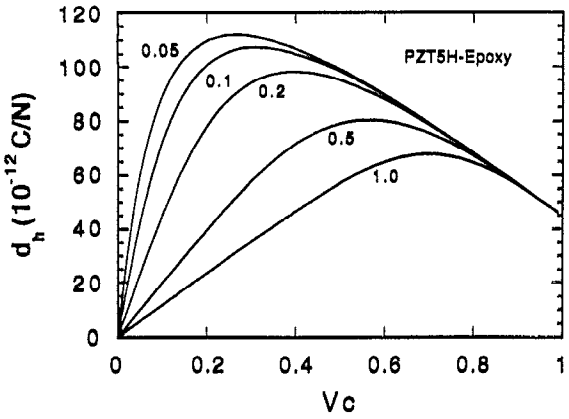

FIG. 5. The hydrostatic piezoelectric constant $\overline{d_h}$ as a function of the ceramic content at a/l ratios of 0.05, 0.1, 0.2, 0.5, and 1.0 for a single-rod PZT5H-epoxy 1-3 composite.

for a PZT5H-epoxy composite using the input data from Table I. $\overline{d_h}$ shows a peak value for each value of a/l; this peak value appears at about 25% for $a/l=0.05$ and shifts to higher ceramic content with the increase of a/l. The peak value increases with the decrease of the ratio a/l; however, there is a saturation of the aspect ratio effect as one can see from Fig. 5. We found that the curve for $a/l=0.05$ is already very close to the saturated value; very little improvement is obtained when the ratio is further decreased to $a/l=0.02$. The curves for $a/l=0.02$ and 0.01 are practically the same.

The 1-3 structure also increases the effective piezoelectric charge constant $\overline{g_h}$ because the effective dielectric constant of the composite is reduced. For hydrostatic applications the conventional criterion for the 1-3 composites is the hydrostatic figure of merit which is defined as $\overline{g_h}\,\overline{d_h}$. For the 1-3 structure, it can be written as follows:

$$\overline{g_h}\,\overline{d_h}=\frac{\overline{d}_h^2}{(\epsilon^c-\epsilon^p)V_c+\epsilon^p} \tag{25}$$

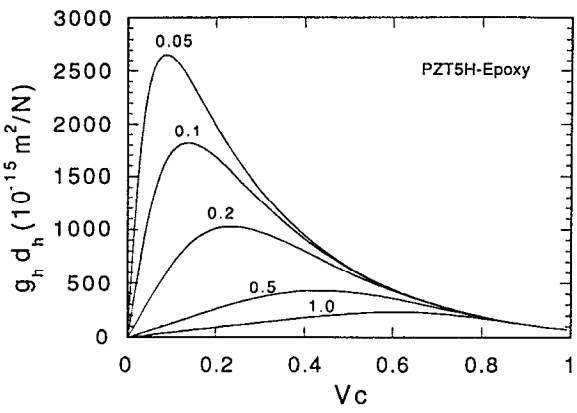

FIG. 6. The figure of merit, $\overline{d_{33}}\,\overline{g_{33}}$, as a function of the ceramic content with the a/l ratios of 0.05, 0.1, 0.2, 0.5, and 1.0, respectively, for a single-rod PZT5H-epoxy 1-3 composite.

Figure 6 is the plot of Eq. (25) as a function of the ceramic content at four different aspect ratios for the PZT5H-epoxy composite using the input data from Table I. One can see that the figure of merit also strongly depends on the ratio a/l. In the commonly used range of the aspect ratio, the hydrostatic figure of merit can be well over 2000×10^{-15} m^2/N for the optimized structure, which is much larger than the conventional piezoelectric ceramics.

III. SOLUTIONS FOR A SINGLE CERAMIC TUBE COMPOSITE

The stress distribution in Fig. 4 tells us that the most useful parts for the stress transfer are those near the ceramic-polymer interface, which suggests that the shape of the ceramic component should be designed to have larger interface area with the polymer. An immediate design possibility would be to replace the ceramic rods with tubes, since for thin wall tubes the interface area can be substantially increased as compared to the solid rods for the same ceramic content. Clearly, from the principle of stress transfer, the structure will be more effective if the interior of the tube is filled with polymer assuming no surface capping. The unit cell for this case is plotted in Fig. 2. In what follows we only give the results for the filled interior tube composite. One can easily derive the solutions for the case of empty interior tube composite following the same procedure.

As shown in the previous section, the hydrostatic case may be treated the same way as the uniaxial case for the 1-3 composite systems. Therefore, we only need to consider the situation of the composite under a uniaxial stress T_3. For the tube composite the unit cell contains three different regions: $r<a_1$; $a_1<r<a_2$; and $a_2<r<R$ as shown in Fig. 2. The surface displacement profiles of the composite in the three regions are, respectively, given by

$$u\left(r,\frac{l}{2}\right)=\begin{cases} A_1 I_0\left(\dfrac{r}{\xi^p}\right)+\dfrac{lT_3}{2Y^p}, & r<a_1, \\ B_1 K_0\left(\dfrac{r}{\xi^p}\right)+B_2 I_0\left(\dfrac{r}{\xi^p}\right)+\dfrac{lT_3}{2Y^p}, & a_2<r<R, \end{cases} \tag{26}$$

$$v\left(r,\frac{l}{2}\right)=C_1 K_0\left(\frac{r}{\xi^c}\right)+C_2 I_0\left(\frac{r}{\xi^c}\right)+\frac{l}{2}s_{33}T_3, \quad a_1<r<a_2\,. \tag{27}$$

The five integration constants in Eqs. (26) and (27) can be obtained using the same boundary conditions as given in Eqs. (6)–(8) at $r=a_1$, a_2, and R, respectively. Because the expressions for these constants are lengthy, we define the following quantities:

$$I_{01}=I_0(a_1/\xi^p),\quad I_{02}=I_0(a_2/\xi^p),\quad I_{11}=I_1(a_1/\xi^p),$$
$$K_{0\bar{1}}=K_0(a_1/\xi^c),\quad I_{0\bar{1}}=I_0(a_1/\xi^c),\quad I_{0\bar{2}}=I_0(a_2/\xi^c),$$
$$I_{1\bar{1}}=I_1(a_1/\xi^c),\quad K_{0\bar{2}}=K_0(a_2/\xi^c),\quad I_{12}=I_1(a_2/\xi^p),$$
$$I_{1\bar{2}}=I_1(a_2/\xi^c),\quad K_{02}=K_0(a_2/\xi^p),\quad K_{12}=K_1(a_2/\xi^p)$$
$$K_{1\bar{1}}=K_1(a_1/\xi^c),\quad K_{1\bar{2}}=K_1(a_2/\xi^c),$$
$$I_{1R}=I_1(R/\xi^p),\quad K_{1R}=K_1(R/\xi^p).$$

In terms of these abbreviations the integration constants in Eqs. (25) and (26) can be written as

$$A_1=\beta[I_{1\bar{1}}(K_{0\bar{1}}-K_{0\bar{2}}-\lambda K_{1\bar{2}})+K_{1\bar{1}}(I_{0\bar{1}}+I_{0\bar{2}}-\lambda I_{1\bar{2}})]T_3, \tag{28}$$

$$B_1=\frac{\beta I_{1R}[R^E I_{01}(I_{1\bar{2}}K_{1\bar{1}}-I_{1\bar{1}}K_{1\bar{2}})+I_{11}I_{1\bar{2}}(K_{0\bar{1}}-I_{0\bar{2}})+I_{11}K_{1\bar{2}}(I_{0\bar{1}}+I_{0\bar{2}})]T_3}{I_{12}K_{1R}-I_{1R}K_{12}}, \tag{29}$$

$$B_2=\frac{\beta K_{1R}[R^E I_{01}(I_{1\bar{2}}K_{1\bar{1}}-I_{1\bar{1}}K_{1\bar{2}})+I_{11}I_{1\bar{2}}(K_{0\bar{1}}-I_{0\bar{2}})+I_{11}K_{1\bar{2}}(I_{0\bar{1}}+I_{0\bar{2}})]T_3}{I_{12}K_{1R}-I_{1R}K_{12}}, \tag{30}$$

$$C_1=\beta[R^E I_{01}I_{1\bar{1}}-I_{11}(I_{0\bar{1}}+I_{0\bar{2}}+\lambda I_{1\bar{2}})]T_3, \tag{31}$$

$$C_2=\beta[R^E I_{01}K_{1\bar{1}}+I_{11}(K_{0\bar{1}}-K_{0\bar{2}}-\lambda K_{1\bar{2}})]T_3, \tag{32}$$

where

$$R^E=\sqrt{c_{44}/s_{33}\mu^p Y^p},\quad \lambda=R^E(I_{1R}K_{02}+I_{02}K_{1R})/(I_{12}K_{1R}-I_{1R}K_{12}),$$

and

$$\beta=\frac{(1/Y^p-s_{33})l/2}{R^E I_{01}(I_{1\bar{1}}K_{0\bar{2}}+\lambda I_{1\bar{1}}K_{1\bar{2}}-\lambda I_{1\bar{2}}K_{1\bar{1}}+K_{1\bar{1}}I_{0\bar{2}})-I_{11}(I_{0\bar{1}}K_{0\bar{2}}+\lambda I_{0\bar{1}}K_{1\bar{2}}+\lambda I_{1\bar{2}}K_{0\bar{1}}-I_{0\bar{2}}K_{0\bar{1}})}.$$

Similar to the previous section, one can find the total charge Q produced at the top surface of the ceramic tube under a uniaxial stress T_3,

$$Q=2\pi\int_{a_1}^{a_2}\frac{2d_{33}}{ls_{33}}v\left(r,\frac{l}{2}\right)r\,dr=\gamma d_{33}T_3\pi(a_2^2-a_1^2), \tag{33}$$

where

$$\gamma=1+\frac{\sqrt{2c_{44}/s_{33}}}{T_3(a_2^2-a_1^2)}[C_1(a_1K_{1\bar{1}}-a_2K_{1\bar{2}})+C_2(a_2I_{1\bar{2}}-a_1I_{1\bar{1}})] \tag{34}$$

is the stress amplification factor for the tube composite under uniaxial stress. One can verify that Eq. (34) recovers the result of Eq. (12) in the limit of $a_1\to 0$.

In Fig. 7 we have plotted Eq. (34) for a single-tube composite of $l=5$ and $R=5$. The ceramic fractions are 0.01, 0.02, 0.05, 0.1, 0.2, and 0.5, respectively, as labeled in the figure. One can see that for each specified ceramic volume percentage the γ value increases with the increase of the inner radius of the tube a_1 at the beginning, then decreases slightly after reaching a peak value. For the 1% ceramic composite, the γ value can be increased by as much as a factor of 2 compared to the ceramic rod composite ($a_1=0$, and for the corresponding 1% ceramic single-rod composite the a/l ratio is 0.1). The slight decrease of γ for large a_1 is caused by the gradual disappearance of the outer interface in the structure, as one can see that the ceramic tube becomes the outer shell for the structure when a_1 is sufficiently large, i.e., $a_2=R$.

Due to the increase of the interface area in the tube ceramic configuration, the effective volume of the polymer that participates in the stress transfer becomes larger. As a result, more charges are produced for the same ceramic content compared with the solid rod composite. In other words, the ceramic tubes are more effective for stress transfer than the solid ceramic rods in the 1-3 composite structure. In principle, other ceramic geometries can also be analyzed in the same manner. However, the displacement field will also depend on the angular variable ϕ for noncylindrical symmetries, which may defy an analytic solution.

IV. SUMMARY AND CONCLUSIONS

A theoretical study has been carried out for the 1-3-type composites based on the model developed in Ref. 6. As examples, a single-rod and single-tube composite have been treated for cylindrical symmetry. Analytic solutions are obtained for the inhomogeneous surface displacements in the z direction under both uniaxial and hydrostatic stress. From these inhomogeneous displacement solutions, the effective piezoelectric constants of 1-3 composites can be calculated.

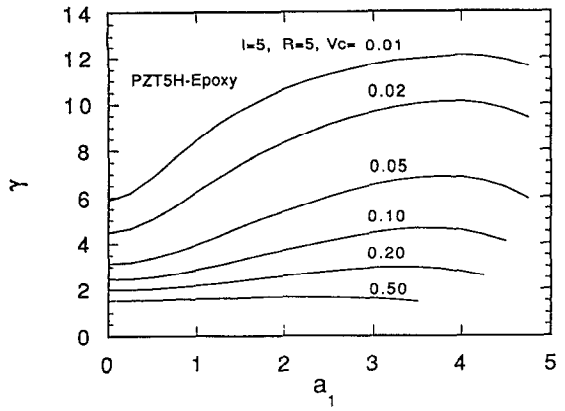

FIG. 7. The change of the amplification factor γ for a single-tube composite with the inner radius of the ceramic tube a_1 for the following volume fractions of ceramic: 0.01, 0.02, 0.05, 0.1, 0.2, and 0.5.

The stress transfer in the 1-3 composites is accomplished through shear coupling at the interface between the two components. Because of the difference in elastic compliance, the two phases cannot have isostrain under uniaxial or hydrostatic stress without surface capping. The effectiveness of the stress transfer can be characterized by a stress amplification factor γ defined in Eqs. (12), (23), and (34). This stress amplification factor is shown to depend on the elastic properties of both phases, the ceramic content, and, more important, the aspect ratio of the ceramic rods. It is shown that the stress transfer effect practically vanishes if the ratio $a/l > 1$. We have also demonstrated that the hydrostatic stress case can be treated in the same way as the uniaxial stress. However, because of the Poisson's ratio effect, the stresses applied in the directions perpendicular to the axial direction of the rod reduces the enhancement effect in the axial direction. Hence, under hydrostatic pressure the amplification factor γ_h is practically reduced by a factor of $(1-2\sigma)$ due to the Poisson's ratio effect, where σ is the Poisson's ratio.

Through the stress analyses, we have shown clearly that the most effective portion of the polymer for the stress transfer is in the vicinity of the ceramic-polymer interface. Therefore, the optimum design for the 1-3 composite structure should contain maximum interface area. If the ceramic volume content and the thickness of the 1-3 structure are fixed, the composite made of ceramic tubes is more effective than the composite made of solid rods due to larger interface area.

In a real 1-3 composite structure the outside boundary of the unit cell is not circular, and the cross section of the ceramic rods may have square or other geometries, for which one must solve each case according to the specified boundary conditions. In general, it may not be possible to obtain closed form expressions, one may have to resort to numerical methods. However, at very low ceramic content, i.e., if the rods are sufficiently far from each other, the single-rod solution obtained here is a very good first-order approximation. Looking at the stress analyses in Fig. 4, we note that the polymer beyond $r=2.5$ actually contributed very little in the stress transfer. This rod distance corresponds to a ceramic volume percentage of about 4%. Therefore, the solutions derived here should be accurate for any rod arrangement if the ceramic content is less than 4%. We have shown that the calculated piezoelectric constant is comparable to the experimental result even for up to 20% ceramic.[10]

Through this theoretical study we have gained substantial insight into the fundamental principles of the 1-3 piezoelectric composite structure, including the mechanism of stress transfer and the influence of the aspect ratio. Several design principles for the 1-3 structure can therefore be stated based on the current study as follows.

(i) The ratio a/l should be relatively small. However, one must note that the enhancement of the stress transfer through reducing the a/l ratio has an upper limit. In the PZT5H-epoxy system (see Fig. 3), if $a/l=0.02$, the γ value essentially reaches the upper limit. Thus, there is no benefit in making the ratio a/l less than 0.02 for this system since the decrease of a/l ratio of the ceramic rods often increases the difficulties in manufacturing 1-3 composites. Using our theoretical results, one can select the design parameters to optimize the performance of 1-3 composites for a specific purpose and at the same time minimize the cost of manufacturing.

(ii) The interface area between the two phases should be maximized so that the effective region of the polymer participating in the stress transfer is maximized.

(iii) From Eq. (14) one may conclude that the passive phase should be chosen to have the smallest possible Young's modulus (depending on the requirement of mechanical strength for the composite) in order to obtain a large γ. In addition, a larger ratio of the shear modulus versus Young's modulus for the passive phase is preferred, which can reduce the self loading of the polymer phase and increase the stress transferred to the ceramic phase. This might be achieved through a surface capping technique.

ACKNOWLEDGMENT

We would like to thank Dr. W. A. Smith for stimulating discussions.

[1] R. E. Newnham, D. P. Skinner, and L. E. Cross, Mater. Res. Bull. **13**, 525 (1978).
[2] D. P. Skinner, R. E. Newnham, and L. E. Cross, Mater. Res. Bull. **13**, 599 (1978).
[3] W. A. Smith, A. Shaulov, and B. A. Auld, in Proceedings of the 1985 IEEE Ultrasonics Symposium, pp. 642–647.
[4] H. L. W. Chan and J. Unsworth, IEEE Trans. Ultrasonics, Ferroelectrics and Frequency Control **UFFC-36**, 434 (1989).
[5] K. A. Klicker, Ph.D. thesis, The Pennsylvania State University, University Park, PA, 1980.
[6] W. Cao, Q. Zhang, and L. E. Cross, IEEE Trans. Ultrasonics, Ferroelectrics and Frequency Control (to be published).
[7] Guide to Modern Piezoelectric Ceramic, from Morgon Matroc, Inc., Vernitron Division.
[8] C. G. Oakley, Ph.D. thesis, The Pennsylvania State University, 1991.
[9] M. J. Haun and R. E. Newnham, Ferroelectrics, **68**, 123 (1986).
[10] Q. Zhang, W. Cao, H. Wang, and L. E. Cross, J. Appl. Phys. (to be published).